Proceedings of the 10th Brazilian Congress of Thermal Sciences and Engineering – ENCIT 2004
Braz. Soc. of Mechanical Sciences and Engineering – ABCM, Rio de Janeiro, Brazil, Nov. 29 – Dec. 03, 2004

Paper CIT04-0524

ONE-EQUATION TURBULENCE MODEL STUDY AND COMPARISON WITH CBS METHOD

Rafael de Mello Pereira
Universidade de Brasília - Departamento de Engenharia Mecânica - Laboratório de Energia e Ambiente - LEA
CEP 70.910-900 - Brasília - DF - Brazil +55(61)307-2314 R236/238
rafaelp@unb.br

Antonio C. P. Brasil Junior
Universidade de Brasília - Departamento de Engenharia Mecânica - Laboratório de Energia e Ambiente - LEA
CEP 70.910-900 - Brasília - DF - Brazil +55(61)307-2314 R236/238
brasiljr@unb.br

Abstract. *This paper present a numerical study of a One-equation turbulence model applied to incompressible flows. The finite element method was used with the Characteristic-based split algorithm, this algorithm use equal order pressure and velocity interpolation and two steps for the pressure coupling. The code implementation use triangular non-structured meshes. The results are compared with other numerical and experimental data for classical test cases like the backward-faced step and the lid-driven cavity.*

keywords: *characteristic-based split, one-equation, turbulence, finite elements*

1. Introduction

The CBS algorithm, coupled with the finite element method, has been used to simulate different kinds of flow regimes, compressible or incompressible (Zienkiewicz and Codina, 1995; O.C. Zienkiewicz and Vàzques, 1995), laminar or turbulent (O. C. Zienkiewicz, 2000b; Massarotti, 1998). This methodology allows the use of equal order interpolation for the pressure and velocity field, and the possibility to stabilize flows for higher local Reynolds (or Peclet) numbers. The stabilization strategy is based in a splitting procedure which treats the pressure term in Navier-Stokes equation as source term computed apart. The semi-implicit form of this algorithm which is presented in this work has a limit time step that controls the stability.

The main idea behind the Characteristic-Based Split method is an operation split which treats the pressure terms of Navier-Stokes equations as source terms. The solution procedure begins solving a transporte equation for each momentum equation without the pressure term. This is reached using a Characteristic-Galerkin procedure (O.C. Zienkiewicz and Nakazawa, 1984; R. Löhner and Zienkiewicz, 1984). The omitted pressure term is used after a pressure change is calculated. For a semi-implicit algorithm a time step restriction is mandatory, in this case the transport problem is full explicit and a time limit based on the mesh size, velocity field and viscosity is calculated.

The Spalart-Allmaras One-Equation turbulence model (Spalart and Allmaras, 1994) is implemented. This model is based on a transport equation for the turbulent viscosity assembled using empiricism, arguments of dimensional analysis and selective dependence on the molecular viscosity. The source term of the transport equation is calculated using the vorticity and a destruction term based in the distance to the wall. The freestream and wall boundary conditions for the turbulence viscosity are trivial and could be implemented using the turbulent viscosity itself.

The Navier-Stokes solver implemented by the use the CBS algorithm is tested with classical laminar cases like the lid-driven cavity and the backward facing step. These cases have been exhaustively explored in the last few decades being perfect validation cases. For the turbulent code a backward faced step geometry is explored and the results are compared with experimental data.

2. Governing Equations

Considering incompressible newtonian flows, the conservation of mass and momentum are expressed by the classical Reynolds averaged equations given by Eq. (1) and Eq. (2).

$$\frac{\partial u_i}{\partial x_i} = 0 \tag{1}$$

$$\frac{\partial \rho u_i}{\partial t} + \frac{\partial \rho u_i u_j}{\partial x_j} = -\frac{\partial p}{\partial x_i} + \frac{\partial}{\partial x_j}\left(\mu \frac{\partial u_i}{\partial x_j} - \rho \overline{u_i' u_j'}\right) \tag{2}$$

In those equations u_i and p corresponds to the mean velocity and pressure fields, ρ and μ corresponds to the density and viscosity of the fluid and $\rho \overline{u_i' u_j'}$ is the Reynolds stress tensor which is modelled by the Boussinesq eddy viscosity assumption given by:

$$\rho \overline{u_i' u_j'} = \frac{2}{3}\rho k \delta_{ij} - 2\mu_T S_{ij} \tag{3}$$

where μ_T is the turbulent eddy viscosity, S_{ij} is the mean rate-of strain tensor and k the kinetic energy of turbulence, defined as:

$$S_{ij} = \frac{1}{2}\left(\frac{\partial u_i}{\partial x_j} + \frac{\partial u_j}{\partial x_i}\right) \tag{4}$$

$$k \equiv \frac{1}{2}\overline{u_i' u_i'} \tag{5}$$

The main feature of the one equation eddy viscosity models is to propose an extra transport equation for ν_T. The model used in the present work is proposed by (Spalart and Allmaras, 1994). In this model the formulation is closed using the following equation for the modified eddy viscosity:

$$\frac{\partial \tilde{\nu}}{\partial t} + u_j \frac{\partial \tilde{\nu}}{\partial x_j} = c_{b1}\tilde{S}\tilde{\nu} + \frac{1}{\sigma}\frac{\partial}{\partial x_j}\left((\nu + \tilde{\nu})\frac{\partial \tilde{\nu}}{\partial x_j}\right) + \frac{c_{b2}}{\sigma}\left(\frac{\partial \tilde{\nu}}{\partial x_i}\frac{\partial \tilde{\nu}}{\partial x_i}\right) - c_{w1} f_w \left(\frac{\tilde{\nu}}{d}\right)^2 \tag{6}$$

In this equation σ, c_{b1}, c_{b2} and c_{w1} are constants, d is the closest distance from the wall, and f_w is a proximity function computed as:

$$f_w = g\left(\frac{1 + c_{w3}^6}{g^6 + c_{w3}^6}\right)^{1/6} \tag{7}$$

with

$$g = r + c_{w2}(r^6 - r), \tag{8}$$

$$r = \frac{\nu_T}{\tilde{S}\kappa^2 d^2}. \tag{9}$$

where

$$\tilde{S} = S + \frac{\tilde{\nu}}{\kappa^2 d^2} f_{\nu 2}, \tag{10}$$

$$f_{\nu 2} = 1 - \frac{\chi}{1 + \chi f_{\nu 1}}, \tag{11}$$

$$f_{\nu 1} = \frac{\chi^3}{\chi^3 + C_{\nu 1}^3}, \tag{12}$$

$$\chi = \frac{\tilde{\nu}}{\nu}. \tag{13}$$

The modified eddy viscosity is defined as

$$\tilde{\nu} = \frac{\nu_T}{f_{\nu 1}} \tag{14}$$

In the present version of the model the deformation rate is measured by the norm of the vorticity tensor, *i. e.*:

$$S = \sqrt{\Omega_{ij}\Omega_{ij}} \tag{15}$$

with

$$\Omega_{ij} = \frac{1}{2}\left(\frac{\partial u_i}{\partial x_j} - \frac{\partial u_j}{\partial x_i}\right) \tag{16}$$

The values of the constants are taken as:

$$C_{b1} = 0.1335, C_{b2} = 0.622, \sigma = 2/3, C_{\nu 1} = 7.1, \tag{17}$$

$$C_{w2} = 0.3, C_{w3} = 2.0, \kappa = 0.41 \tag{18}$$

3. Numerical Methods

The basis of CBS algorithm is the computation of multiple steps in an incremental integration. This approach can assure the stability for the pressure and velocity discretization as well as for the local Reynolds number. The analysis of this approach is explored in many articles (Zienkiewicz and Codina, 1995; O.C. Zienkiewicz and Vàzques, 1995) and in particular for CBS algorithm in (O. C. Zienkiewicz, 2000b or R. Codina and Zienkiewicz, 1998).

To solve the conservation equations (1), (2) and (6), the following steps are used:

1. given initial conditions ($u_i^{t=0}$,ν_T^0)
2. Step 1: Solve velocity field with Characteristic-Galerkin procedure.

$$\Delta u_i^* = u_i^* - u_i^n = \Delta t \left[-\frac{\partial}{\partial x_j}(u_j u_i) + \frac{1}{\rho}\frac{\partial}{\partial x_j}\left((\mu + \mu_T)\frac{\partial u_i}{\partial x_j} \right) + \frac{\Delta t}{2} u_k \frac{\partial}{\partial x_k}\left(\frac{\partial}{\partial x_j}(u_j u_i) \right) \right]^n \tag{19}$$

3. Step 2: Solve pressure equation for Δt

$$\Delta t \frac{\partial^2 \Delta p}{\partial x_i \partial x_i} = \frac{1}{\theta_1}\frac{\partial U_i^n}{\partial x_i} + \frac{\partial \Delta U_i^*}{\partial x_i} - \Delta t \left(\frac{\partial^2 p^n}{\partial x_i \partial x_i} \right) \tag{20}$$

where $0.5 \leq \theta_1 \leq 1$ for the semi-implicit form.

4. Step 3: Solve velocity correction

$$\Delta u_i = u_i^{n+1} - u_i^n = \Delta u_i^* - \Delta t \frac{\partial p^{n+1}}{\partial x_i} \tag{21}$$

5. Step 4: Solve Eddy viscosity transport equation to calculate the new turbulent viscosity.

$$\Delta \tilde{\nu} = -\Delta t \left[\frac{\partial (u_j \tilde{\nu})}{\partial x_j} - \frac{\partial}{\partial x_i}\left(k \frac{\partial \tilde{\nu}}{\partial x_i} \right) + Q \right]^n + \frac{\Delta t^2}{2} u_k^n \frac{\partial}{\partial x_k} \left[\frac{\partial (u_j \tilde{\nu})}{\partial x_j} - \frac{\partial}{\partial x_i}\left(k \frac{\partial \tilde{\nu}}{\partial x_i} \right) + Q \right]^n \tag{22}$$

where Q is the source term calculate using the old velocity and viscosity values:

$$Q = c_{b1} \tilde{S} \tilde{\nu} + \frac{c_{b2}}{\sigma}\left(\frac{\partial \tilde{\nu}}{\partial x_i}\frac{\partial \tilde{\nu}}{\partial x_i} \right) - c_{w1} f_w \left(\frac{\tilde{\nu}}{d} \right)^2 \tag{23}$$

For all the equations given above the Galerkin spatial discretization is applicable without stability problems, the details concerning this spatial discretization can be found in any basic finite elements biography (O. C. Zienkiewicz, 2000a; Hughes J.R., 1986). The Galerkin method application in the above equation leads to following weak form for the equations (19; 20;21):

$$\begin{aligned} \int_\Omega N_u^k \Delta u_i^* d\Omega = & \\ & = +\Delta t \left[-\int_\Omega N_u^k \frac{\partial}{\partial x_j}(u_j u_i) d\Omega - \int_\Omega \frac{\partial N_u^k}{\partial x_j}\left((\nu + \nu_T)\frac{\partial u_i}{\partial x_j} \right) d\Omega \right]^n \\ & + \frac{\Delta t^2}{2} \left[\int_\Omega \frac{\partial}{\partial x_l}(u_l N_u^k) \left(-\frac{\partial}{\partial x_j}(u_j u_i) \right) d\Omega \right]^n \\ & + \Delta t \left[\int_\Gamma N_u^k \left((\nu + \nu_T)\frac{\partial u_i}{\partial x_j} \right) n_j d\Gamma \right]^n \end{aligned} \tag{24}$$

where N_u is the standard finite element shape function.

$$\Delta t \int_\Omega \frac{\partial N_p^k}{\partial x_i} \left[u_i^n + \theta_1 \left(\Delta u_i^* - \Delta t \frac{\partial p^{n+1}}{\partial x_i} \right) \right] d\Omega - \Delta t \theta_1 \int_\Gamma N_p^k \left(u_i^n + \Delta u_i^* - \Delta t \frac{\partial p^{n+1}}{\partial x_i} \right) n_i d\Gamma = 0 \tag{25}$$

$$\begin{aligned} \int_\Omega N_u^k \Delta u_i^{n+1} d\Omega = & \int_\Omega N_u^k \Delta u_i^* d\Omega \\ & -\Delta t \int_\Omega N_u^k \left(\frac{\partial p^n}{\partial x_i +} + \frac{\partial \Delta p}{\partial x_i} \right) d\Omega - \frac{\Delta t^2}{2} \int_\Omega \frac{\partial}{\partial x_j}(u_j N_u^k) \frac{\partial p^n}{\partial x_i} d\Omega \end{aligned} \tag{26}$$

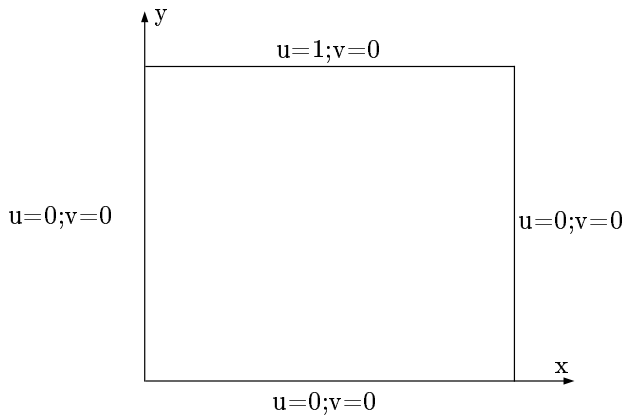

Figure 1: Cavity Geometry and Boundary Conditions

The equations above are solved using a triangular unstructured mesh. The solution of the transport equation in the first and the last steps are carried out explicitly using a lumped mass matrix (O. C. Zienkiewicz, 2000a) for simplicity. The solution of the linear system of equation that appears in the pressure evaluation is achieved using a conjugated gradients method.

4. Laminar Results

In this section two numerical examples are presented in order to validate the laminar code. The two studied problems are classical benchmark cases that have been studied for years.

4.1. Lid-Driven Cavity Flow

This case is widely used in the validation of Navier-Stokes solvers. Figure (1) shows the geometry and boundary conditions used. A node pressure restriction is also used in the middle of the bottom corner. The main challenge concerning this problem is existence of the two singularities where the cavity walls met the cavity lid. This type of corner singularities are very usual in real world problems. A mesh of 40 x 40 elements with a geometric concentration factor is used in this example. Four conditions of flow are simulated with Re= 100, 200, 400 and 1000.

Figure (2) shows a good agreement between the results simulated and those obtained with more refined grids (Akin, 1994; Ghia and K. N. Ghia, 1982). Concerning this problem as the Reynolds number increases the vortex move away from the driving wall toward the geometric center of the cavity, while new small vortex are formed at the corners. The velocity field is well developed and smooth in all the domain. The vortex behavior is very similar to that observed in the cited bibliography reference. The results can be considered to be very satisfactory.

4.2. Laminar Backward-Facing Step Problem

Many usual engineering applications have recirculation zones. To test and validate CFD codes over these recirculation conditions the backward-facing step case has been used for years. Figure (3) shows the geometries used. The boundary conditions adopted are an inlet parabolic u velocity profile together with a zero vertical velocity v. Non-slip conditions are enforced on all solid walls. For the out-flow a Neumann condition is imposed with a zero pressure restriction. Two different geometries are used:

- Geometry 1: H=1.5, h=1.0, L=22, e l=3
- Geometry 2: H=1.0, h=0.5, L=22, e l=3

Altogether four cases are simulated with two Reynolds number Re=50 and 150 being used for each geometry.

1. Geometry (1), Re=50, mesh with 2017 nodes and 3840 elements.

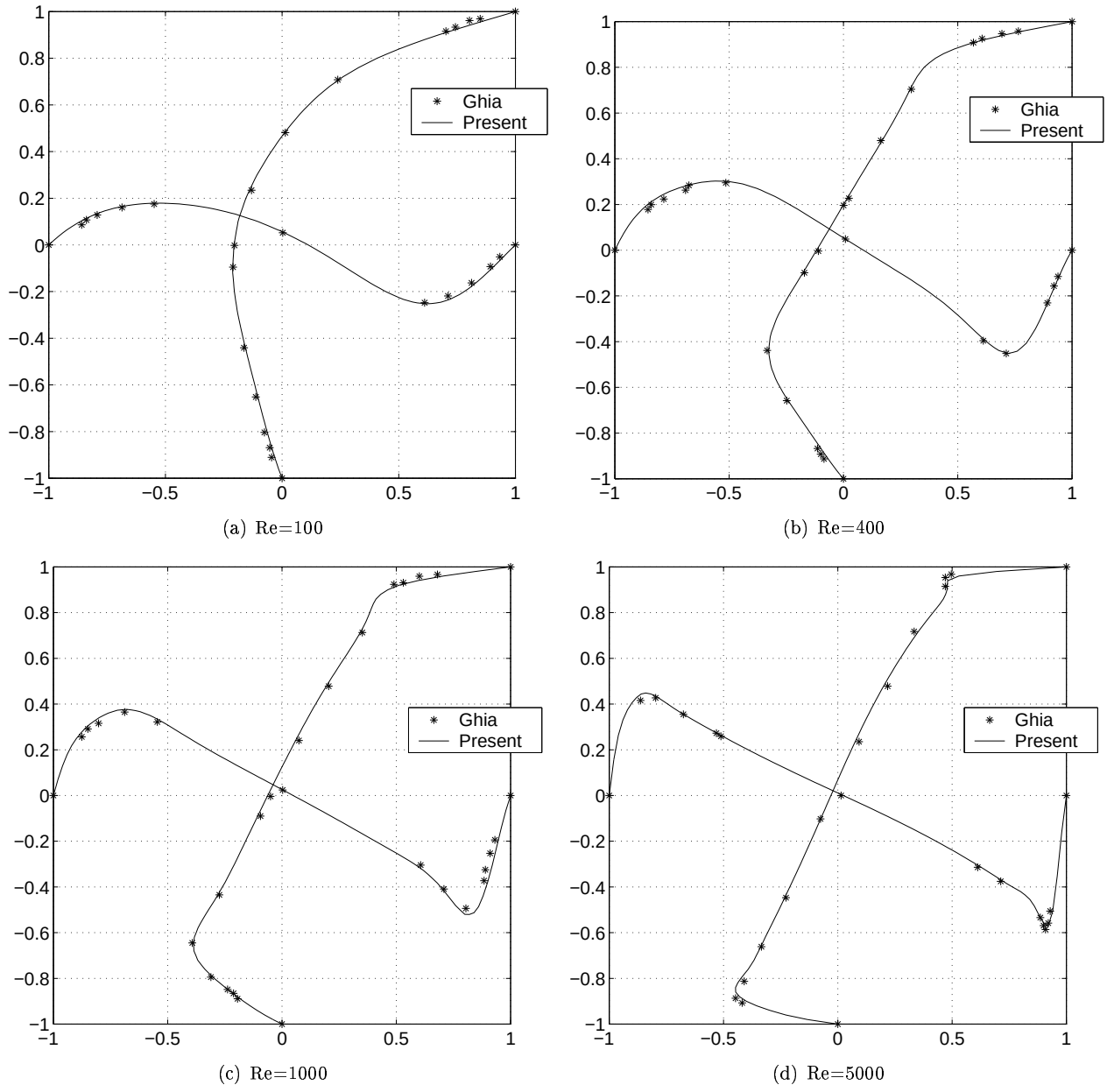

(a) Re=100 (b) Re=400

(c) Re=1000 (d) Re=5000

Figure 2: Middle velocity profiles for the cavity

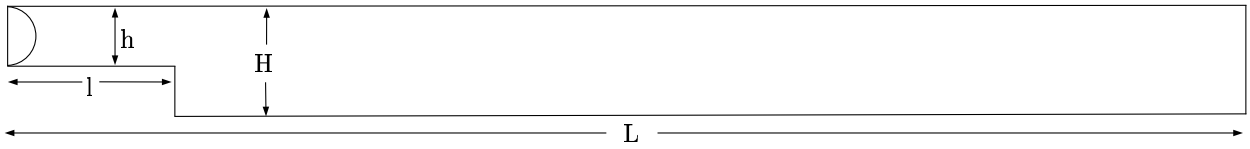

Figure 3: Backward-facing step geometry.

2. Geometry (2), Re=50, mesh with 2017 nodes and 3840 elements.
3. Geometry (1), Re=150, mesh with 2017 nodes and 3840 elements.
4. Geometry (2), Re=150, mesh with 2017 nodes and 3840 elements.

The Reynolds number is defined by:

$$Re = \frac{|\mathbf{U_{max}}| \cdot (H - h)}{\nu} \tag{27}$$

The results obtained show that the velocity is well developed over all the domain. The big recirculation zone at the step bottom, that is the main characteristic of this problem, is also present. The predicted results agree quite well with the results obtained for many researchers (Morgan et al., 1982). A comparison with some of these results show a suitable agreement of the reattachment point and maximum and minimum velocity. Those comparisons are shown in Tables (1; 2; 3; 4).

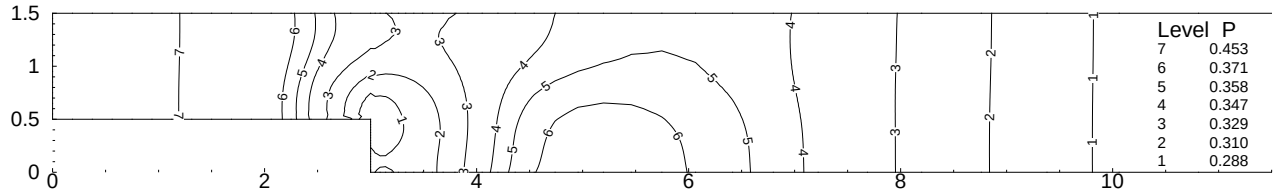

Figure 4: Pressure field for laminar step, case 1.

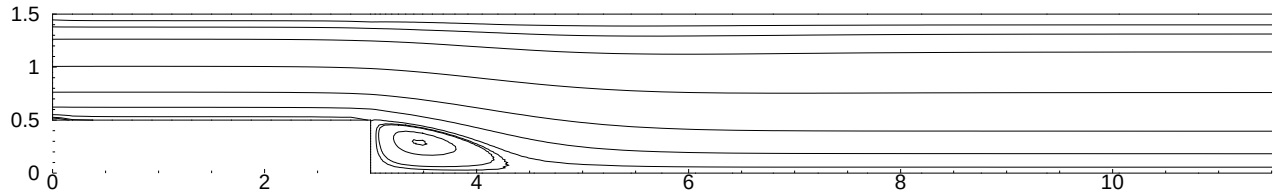

Figure 5: Streamlines for laminar step, case 1.

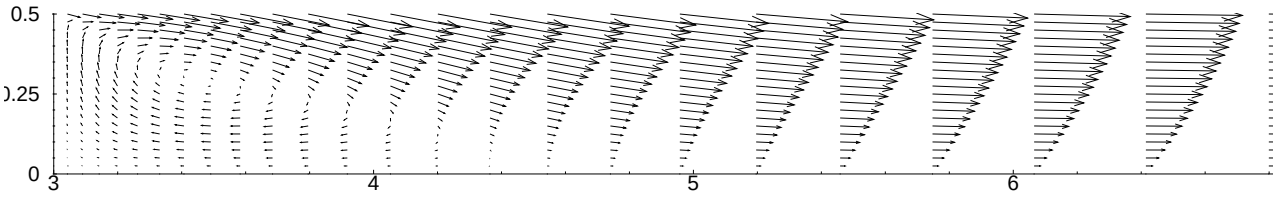

Figure 6: Recirculation zone detail for laminar step, case 1.

Table 1: u velocity ,d=1.6 (after the step)

Resultados	Case i		Case ii		Case iii		Case iv	
	Min.	Max.	Min.	Max.	Min.	Max.	Min.	Max.
Present	-0.05	0.91	-0.04	0.71	-0.07	0.97	-0.10	0.90
Kueny-Binder	-0.04	0.90	–	–	-0.07	0.97	-0.09	0.92
Buffat et. al.	-0.05	0.89	-0.02	0.69	-0.07	0.95	-0.11	0.88
Dhatt-Hubert	-0.05	0.86	-0.05	0.74	-0.06	0.96	-0.10	0.91
Donea et. al.	-0.06	0.91	-0.06	0.73	-0.08	0.97	-0.10	0.90
Ecer et. al.	-0.06	0.91	-0.06	0.72	-0.09	0.92	-0.04	0.87
Glowinski et. al.	-0.04	0.91	-0.03	0.71	-0.07	0.96	-0.10	0.90
Hecht	-0.05	0.91	-0.04	0.72	-0.07	0.97	-0.103	0.90

Table 2: u velocity ,d=4 (after the step)

Resultados	Case i		Case ii		Case iii		Case iv	
	Min.	Max.	Min.	Max.	Min.	Max.	Min.	Max.
Present	0.00	0.78	0.00	0.52	-0.05	0.91	-0.045	0.72
Kueny-Binder	0.00	0.72	–	–	-0.05	0.93	-0.016	0.71
Buffat et. al.	0.00	0.77	0.00	0.52	-0.05	0.90	-0.03	0.70
Dhatt-Hubert	0.00	0.78	0.00	0.52	-0.03	0.91	-0.04	0.72
Donea et. al.	0.00	0.78	0.00	0.53	-0.06	0.91	-0.06	0.72
Ecer et. al.	0.00	0.77	0.00	0.53	-0.03	0.87	-0.03	0.71
Glowinski et. al.	0.00	0.77	0.00	0.52	-0.05	0.91	-0.05	0.72
Hecht	0.00	0.78	0.00	0.52	-0.05	0.91	-0.05	0.73

Table 3: u velocity ,d=8 (after the step)

Resultados	Case i		Case ii		Case iii		Case iv	
	Min.	Max.	Min.	Max.	Min.	Max.	Min.	Max.
Present	0.00	0.69	0.00	0.50	0.00	0.81	0.00	0.56
Kueny-Binder	–	–	–	–	0.00	0.82	0.00	0.56
Buffat et. al.	0.00	0.69	0.00	0.50	0.00	0.80	0.00	0.54
Dhatt-Hubert	0.00	0.69	0.00	0.50	0.00	0.81	0.00	0.56
Donea et. al.	0.00	0.69	0.00	0.50	0.00	0.82	0.00	0.55
Ecer et. al.	0.00	0.69	0.00	0.51	0.00	0.79	0.00	0.51
Glowinski et. al.	0.00	0.69	0.00	0.50	0.00	0.80	0.00	0.56
Hecht	0.00	0.70	0.00	0.50	0.00	0.81	0.00	0.56

Table 4: Reattachment point after the step

Resultsr	Case(i)	Case(ii)	Case(iii)	Case(iv)
Present	3.0	2.1	6.8	4.9
Kueny-Binder	3.0	–	6.0	4.5
Buffat et. al.	2.5	1.0	5.8	4.5
Dhatt-Hubert	3.0	2.0	6.5	5.0
Donea et. al.	2.5	2.0	6.0	5.0
Ecer et. al.	3.0	2.8	5.9	4.7
Glowinski et. al.	2.5	1.8	4.8	4.4
Hecht	2.76	2.1	6.0	4.6

5. Flow over a Turbulent Backward-facing step

This problem has served as a benchmark for experimental and numerical studies for years. The results obtained are compared with (Kim, 1978) and other reference work for this case is (Ross and Larock, 1997).

The geometry utilized is the same used for the laminar case Fig. (3) with the follow dimensions:

- Geometry: H=3.0, h=1.0, L=20, e l=3

The boundary conditions adopted are an inlet full developed velocity and turbulence profile, these profile is previously calculated using the same numerical code and a channel-flow. The inlet velocity profile used agrees with (Wilcox, 1994). Non-slip conditions are enforced on all solid walls. For the out-flow a Neumann condition is imposed with a zero pressure restriction. A Reynolds number of 47,000 is used in this case. The mesh utilized has 3279 nodes and 6320 triangular elements Fig (7). The mesh is refined close to the step in the recirculation zone.

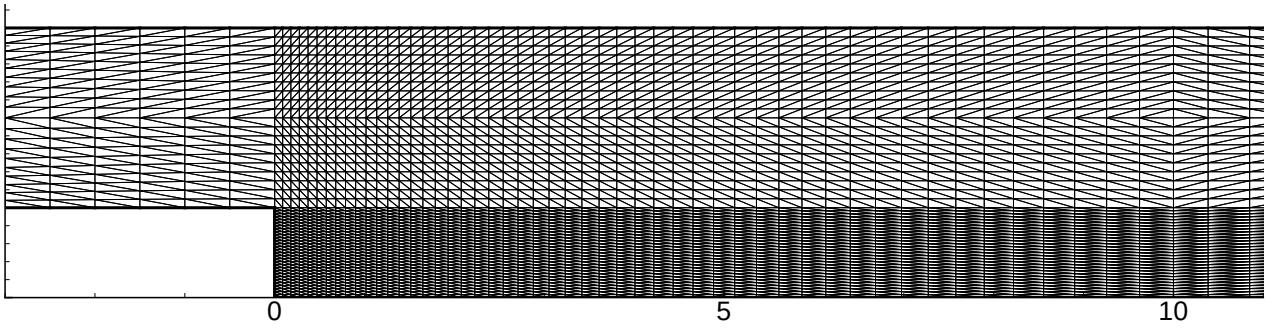

Figure 7: Mesh used for the turbulent step case

The velocity and pressure fields found are well developed and smooth in all domain as shown in the Figures (9; 10; 11). The erros and discontinuities in the velocity and pressure field are insignificant. The comparison of the velocity profiles with experimental results (Kim, 1978) for four different positions along the step are shown in Fig. (8). These positions are taken based in the step height and for this case 1.5,2,5.5,10.5. The characteristic big recirculation zone is presente, and beneath this one a small recirculation also appears Fig. 11.

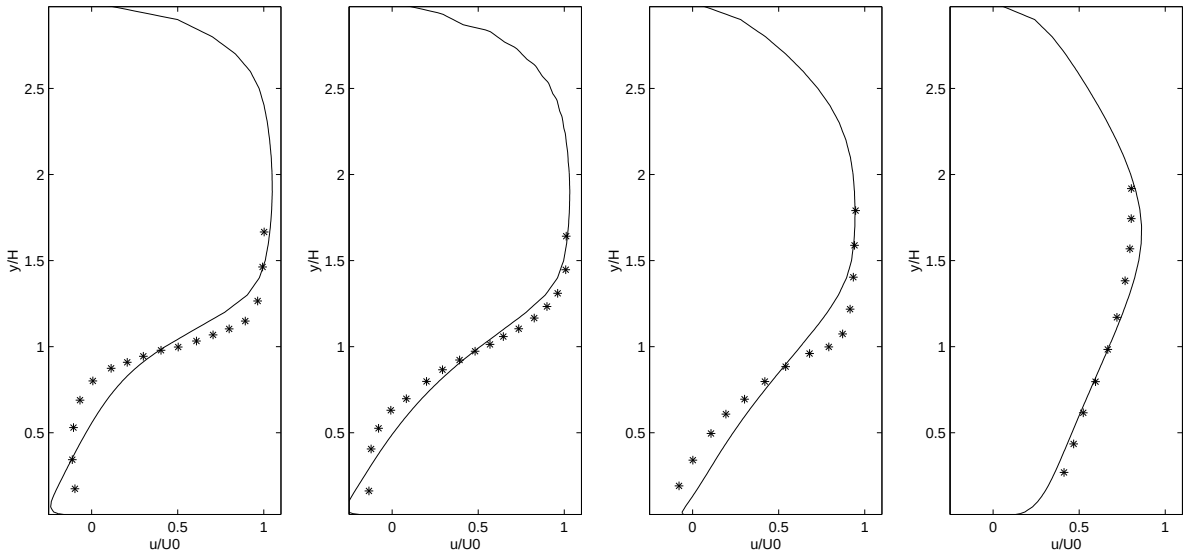

(a) d=1.5 (b) d=2 (c) d=5.5 (d) d=10.5

Figure 8: Step velocity profile, (* Experimental) ; (— Numerical)

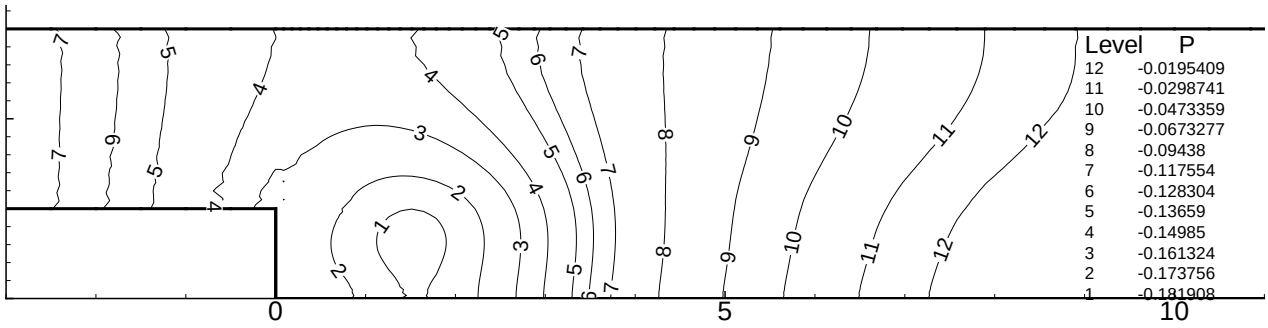

Figure 9: Pressure field for turbulent step.

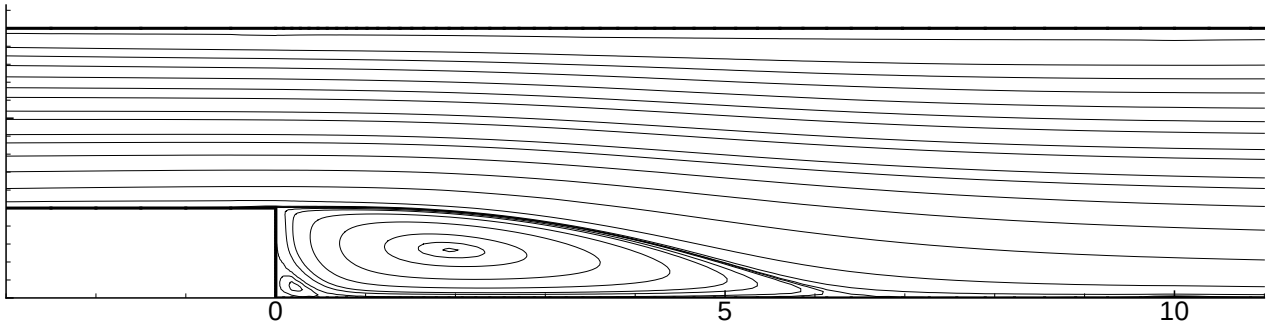

Figure 10: Streamlines for turbulent step.

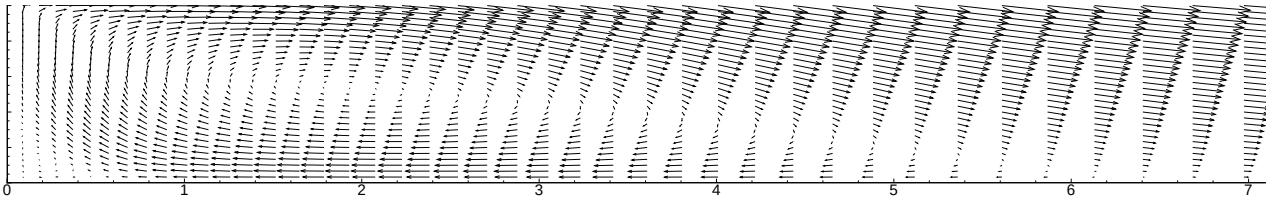

Figure 11: Recirculation zone detail for turbulent step.

6. Conclusions

The CBS code implemented has a very stable behavior. In all studied cases the convergence was reached without considerable residual oscillation. An implementation advantage of this code perceived is the same interpolation order for pressure and velocity. This is very significant as long as only one mesh has to be generated and the velocity and pressure unknowns can be evaluated at the same mesh points. Other computacional advantage concerning this algorithm is that the sparse system of equations is symmetric and positive definite and can be solved using the very efficient conjugated gradients method.

The two classical laminar cases studied presented a reasonable agreement with the vast bibliography existent. The cavity flow was solved for moderated high Reynolds numbers using not so fine mesh and the results obtained coincide with the results using finite difference and more fine grids (Ghia and K. N. Ghia, 1982). The backward-faced step case results are close to those obtained in the workshop (Morgan et al., 1982). The cavity and backward-facing step flows are good challenger for numerical codes. Both flows examples were used in order to validade the present numerical code.

The turbulent code show good results for its simplicity and easy implementation. The convergence was reached easily and without any numerical oscillation. The computational time was very compatible with the laminar case.

7. Acknowledgements

The authors would like to acknowledge the financial support of Eletronorte S.A and CNPq.

8. References

Akin, J. E., 1994, "Finite Elements for Analysis and Design", Academic Press Limited, 24-28 Oval Road London NW1 7DX.

Ghia, U. and K. N. Ghia, C. T. S., 1982, High-Re Solution for Incompressble Flow Using the Navier-Stokes Equation and a Multigrid Method, "J. Comp. Physics", Vol. 48, pp. 387–411.

Hughes J.R., Mallet Michel, M. A., 1986, A new Finite Element Formulation for Computational Fluid Dynamics: II. Beyond SUPG, "Computer Methods in Applied Mechanics and Engineering", , No. 54, pp. 341–355.

Kim, J. S., 1978, "Investigation of separation and reattachment of a turbulent shear layer: lfow over a backward-facing setp", PhD thesis, Stanford University.

Massarotti, N., 1998, Characteristic-based-split (CBS) algorithm for incompressible flow problems flow problems with heat transfer, "Int. J. Num. Meth. Fluids.", Vol. 8, pp. 969–990.

Morgan, K., Periaux, J., and Thomasse, F., 1982, Analysis of Laminar Flow over a Backward Facing Step, "A GAMM-Workshop".

O. C. Zienkiewicz, R. T., 2000a, "The Finite Element Method: Basics", Vol. 1, Butterworth-Heinemann, Linacre House, Jordan Hill, Oxford OX2 8DP.

O. C. Zienkiewicz, R. T., 2000b, "The Finite Element Method: Fluid Dynamics", Vol. 3, Butterworth-Heinemann, Linacre House, Jordan Hill, Oxford OX2 8DP.

O.C. Zienkiewicz, R. Löhner, K. M. and Nakazawa, S., 1984, Finite elements in fuid mechanics - a decade of progress, "Finite elements in fluids", Vol. 5, pp. 1–26.

O.C. Zienkiewicz, B.V.K.S Sai, K. M. R. C. and Vàzques, M., 1995, A general algorithm for compressible and incompressible flow- Part II. Testes on the explict form., "Int. J. Num. Meth Fluids", Vol. 20, pp. 1061–1080.

R. Codina, M. V. and Zienkiewicz, O., 1998, A fractional step method for the solution of compressible Navier-Stokes equations, "Computational Fluid Dynamics Review", Vol. 1, pp. 331–347.

R. Löhner, K. M. and Zienkiewicz, O., 1984, The solution of non-linear hyperbolic equation systems by the finite elements method, "Int. J. Num. Meth. Fluids", Vol. 4, pp. 1043–1063.

Ross, J. A. and Larock, B. E., 1997, An Algebric Stress Finite Element Model of Turbulent Flow, "International Journal for Numerical Methods in Fluids".

Spalart, P. R. and Allmaras, S. R., 1994, A one-equation turbulence model for aerodynamic flows, "La Recherche Aérospatiale".

Wilcox, D. C., 1994, "Turbulence Modeling for CFD", DCW Industries.

Zienkiewicz, O. and Codina, R., 1995, A general algorithm for compressible and incompressible flow. Part I. The split characteristic based scheme., "Int. J. Num. Meth. Fluids", Vol. 20, pp. 869–885.